

## Structural fluctuations in NbO<sub>2</sub> at high temperatures

R. Pynn\* and J. D. Axe

*Physics Department, Brookhaven National Laboratory, Upton, New York 11973*

P. M. Raccah

*Department of Physics, University of Illinois, Chicago Circle, Chicago, Illinois 60680*

(Received 21 October 1977)

Inelastic neutron scattering has been used to study the fluctuations associated with the structural phase transformation at  $T_c = 808.5^\circ\text{C}$  in NbO<sub>2</sub>. Above  $T_c$  there is strong quasielastic scattering centered upon the reciprocal-lattice position  $\bar{q}_p = (\frac{1}{4}, \frac{1}{4}, \frac{1}{2})$ , but lying along rods oriented parallel to (110) directions. The temperature dependence of the anisotropic correlation lengths and energy widths have been determined. We show that the structural fluctuations consist of strongly-coupled antiferrodistortive distortions within (110) planes in the parent rutile structure with much weaker correlations of the fluctuations from plane to plane. A simple mean-field pseudospin treatment can be used to discuss the data semiquantitatively and aids in understanding the relationship between the structural instabilities in NbO<sub>2</sub> and its isoelectronic compound VO<sub>2</sub>. No evidence was found for a soft-phonon branch.

### I. INTRODUCTION

The metal-insulator phase transformation in vanadium dioxide (VO<sub>2</sub>) has been the subject of numerous studies since it was first observed over two decades ago,<sup>1</sup> and a considerable fraction of our current understanding of real metal-insulator systems derives from these studies. By comparison, the phase transformation in the isoelectronic compound niobium dioxide (NbO<sub>2</sub>) has received scant attention. This is due in part to a more extreme transformation temperature ( $T_c \approx 810^\circ\text{C}$  for NbO<sub>2</sub> compared with  $\approx 67^\circ\text{C}$  for VO<sub>2</sub>) which delayed its discovery,<sup>2,3</sup> and in part to the fact the electrical transport properties of NbO<sub>2</sub>, while anomalous near  $T_c$ ,<sup>1-4</sup> are not as dramatic as in VO<sub>2</sub>. In spite of these differences the phase transformations in the two compounds are closely related from a structural point of view. Both materials have the same high-temperature rutile structure (tetragonal space group  $D_{4h}^{14}$ ) with two formula units per cell (see Fig. 1). The low-temperature insulating phases, on the other hand, have distinctly different structures. VO<sub>2</sub> is monoclinic<sup>5</sup> ( $C_{2h}^5$ , with four formula units per cell), while NbO<sub>2</sub> is body-centered tetragonal ( $C_{4h}^6$ ) with a primitive cell containing sixteen formula units.<sup>6</sup> These differences are, however, superficial. A careful comparison of the structural distortions which accompany the phase transformations shows a number of common features and provides fresh insight into the nature of the instabilities in both materials.<sup>7,8</sup>

The NbO<sub>2</sub> phase transformation is more amenable to study by neutron diffraction than is the one in VO<sub>2</sub>.

Vanadium nuclides scatter neutrons (predominantly) incoherently while the interesting structural changes at the phase transformations must be studied by coherent scattering. A series of studies<sup>7-10</sup> of the latter type with NbO<sub>2</sub> has established the following principal facts.

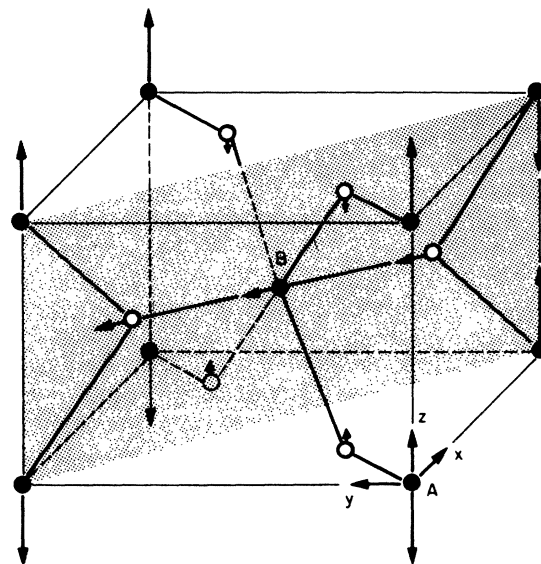


FIG. 1. High-temperature unit cell of NbO<sub>2</sub> with the displacements due to the  $\bar{q}_A$  distortion indicated by arrows. The A and B metal sublattices are indicated. (●, Nb; ○, oxygen)

(i) As a consequence of the increased size of the unit cell of low-temperature (LT) NbO<sub>2</sub>, a series of "superlattice" Bragg reflections appear below  $T_c$ . Shapiro *et al.*<sup>9</sup> showed that the intensities of these reflections appear to go to zero in a continuous manner at  $T_c$ , indicating that the transformation is of second order. They showed that in the vicinity of specific superlattice reflections there is diffuse quasi-elastic scattering which persists even above  $T_c$ . The present paper is primarily a study of the nature of this diffuse scattering and of the short-range structural correlations which cause it.

(ii) Shapiro *et al.*<sup>9</sup> noted that the principal atomic displacements associated with the transformation could be represented as the sum of plane waves

$$\bar{u}_{lk} = \sum_{\{\bar{q}_p\}} \eta_p(T) \bar{\xi}_k(\bar{q}_p) \exp[i\bar{q}_p \cdot \bar{r}(lk)] \quad (1)$$

where  $\bar{r}(lk)$  is the position of the  $k$ th atom of the  $l$ th unit cell of the high-temperature (HT) rutile phase and  $\bar{u}_{lk}$  is the displacement of this atom in the low-temperature (LT) phase.  $\{\bar{q}_p\}$  represents a set of four symmetry-related wave vectors belonging to the same "star." Specifically,  $\bar{q}_p \equiv \{\pm \bar{q}_A, \pm \bar{q}_B\}$ , where  $\bar{q}_A = (\frac{1}{4}, -\frac{1}{4}, \frac{1}{2})$  and  $\bar{q}_B = (\frac{1}{4}, \frac{1}{4}, \frac{1}{2})$  are shown in Fig. 2. The temperature-dependent amplitudes  $\eta_p(T)$  can be taken as the order parameters for the transformation. Shapiro *et al.* discussed this transformation in terms of a "soft phonon mode" instability although a cursory search failed to reveal a well-defined phonon branch with  $\omega(\bar{q}_p, T_c) \rightarrow 0$ .

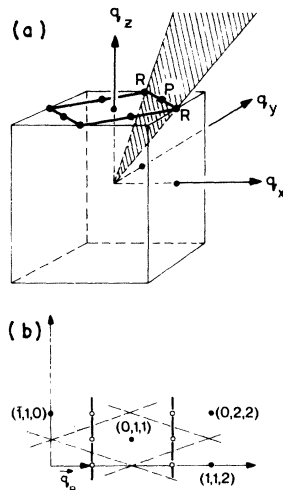


FIG. 2. (a) Reciprocal lattice of the HT phase with the scattering plane of the present experiment shaded. (b) Scattering plane showing HT Bragg points (●),  $P$  points (○), and rods of critical scattering (heavy lines). The dashed lines are Brillouin-zone boundaries which intersect the rods of scattering at  $R$  points.

(iii) In Refs. 7 and 8, Pynn *et al.* refined the atomic positional parameters of the LT phase using conventional neutron crystallography and showed that the  $\bar{\xi}_k$  of Eq. (1) transformed as a single irreducible representation of the group of  $\{\bar{q}_p\}$ . The displacements associated with  $\pm \bar{q}_A$  are shown exaggerated but on a correct relative scale in Fig. 1. This figure also defines two interpenetrating  $A$  and  $B$  sublattices of metal atoms. As discussed by Pynn *et al.*, the LT distortion associated with  $\bar{q}_A$  can be characterized as a dimerization of  $A$  sublattice metal atoms in chains along the [001] direction, together with movement of the  $B$  sublattice atoms in the [110] direction and some concomitant displacements of the oxygen atoms. The displacements associated with  $\pm \bar{q}_B$  are related to those shown in Fig. 1 by a four-fold screw axis which interchanges the  $A$  and  $B$  metal sublattices. Secondary displacements involving other wave vectors [ $\bar{q}_M \equiv (\frac{1}{2}, \frac{1}{2}, 0)$ ,  $\bar{q}_X \equiv (\frac{1}{2}, 0, 0)$  and  $\bar{q}_I \equiv (0, 0, 0)$ ] are necessary for a complete description of the LT phase. These displacements, which result from nonlinear coupling to the primary  $\{\bar{q}_p\}$  displacements, were shown by Pynn *et al.* to be small and they will not be considered further in this paper.

(iv) The structural distortions accompanying the phase transformation in VO<sub>2</sub> are based upon a different set of wave vectors  $\{\bar{q}_R\} \equiv \{\frac{1}{2}, 0, \frac{1}{2}\}$  (see Fig. 2), but it is once again possible to distinguish degenerate "modes" which dimerize the  $A$  and  $B$  sublattices, respectively.<sup>10</sup> Axe *et al.*<sup>8</sup> pointed out that when viewed in this way, the individual sublattice-distortion patterns of NbO<sub>2</sub> and VO<sub>2</sub> are similar. Both materials are composed of (110) planes within which adjacent  $c$ -axis chains of metal atoms are dimerized in an out-of-phase or antiferrodistortive manner. (The shaded region in Fig. 1 defines such a plane for the  $A$ -sublattice distortions in NbO<sub>2</sub>.) The NbO<sub>2</sub> and VO<sub>2</sub> structures differ only in the phase relationship of the dimerization patterns in neighboring (110) planes. The present study shows that these planar correlations persist well above  $T_c$  in NbO<sub>2</sub>.

## II. EXPERIMENTAL PROCEDURES AND RESULTS

The NbO<sub>2</sub> single crystal used in these experiments was prepared by melting stoichiometric amounts of Nb metal (99.99% purity) and Nb<sub>2</sub>O<sub>3</sub> (99.95% purity) which had previously been reacted in a carbon crucible under argon. The boule was pulled from the melt by the conventional Czochralski method using a tungsten pulling rod and a pulling rate of  $\sim 1$  cm/h.<sup>11</sup> Chemical analysis indicates that this technique produces crystals with a slight oxygen deficiency, NbO<sub>1.9976 ± 0.0008</sub>. Neutron diffraction showed the lower half of the boule to be a single crystal, with a mosaic spread  $\sim 0.5^\circ - 0.7^\circ$  of arc. After removal of the upper polycrystalline por-

tion the resulting sample was roughly cylindrical, 8 mm in diameter and 17 mm high, with the cylinder axis approximately coincident with the crystallographic  $c$  axis. The present sample has about four times the volume of the one used by Shapiro *et al.*<sup>9</sup> in their neutron scattering study. The room-temperature lattice constants referred to the HT rutile cell are in good agreement with those given by Marinder,<sup>6</sup>  $a_R = 4.846 \text{ \AA}$  and  $c_R = 2.993 \text{ \AA}$ .

During the measurements the sample was heated in a tungsten-mesh vacuum oven with temperature control of about  $\pm 1 \text{ }^\circ\text{C}$ . The neutron scattering measurements were performed on three-axis spectrometers at the Brookhaven High Flux Beam Reactor. For reasons which will later become clear, the sample was mounted in an unconventional geometry with a scattering plane which contained both the  $(1,1,2)$  and  $(\bar{1}, 1, 0)$  reciprocal-lattice vectors, as shown in Fig. 2. Studies involving energy transfers of less than 2 meV were done with a curved pyrolytic-graphite(002) monochromator and a plane analyzer of the same material. Oriented graphite filters were used to remove order contamination in the incident 14-meV beam. Measurements involving larger energy transfers (phonon searches) used either a graphite(002) monochromator with the incident neutron energy fixed at 40 meV or a Be(002) monochromator with the scattered neutron energy fixed at 40 meV. In all cases the collimation was adjusted to meet the needs of the experiment. By observing the temperature dependence of the superlattice intensities  $T_c$  was estimated to be  $808.5 \text{ }^\circ\text{C}$  ( $\pm 1 \text{ }^\circ\text{C}$ ), which is in good agreement with other recent determinations.<sup>9,12</sup>

#### A. Search for a "soft phonon"

Because of the increased sample size, it was deemed worthwhile to renew the search begun by Shapiro *et al.*,<sup>9</sup> for a phonon mode with a well-defined frequency and an eigenvector similar to that of the condensed displacements. In the simplest "soft-phonon" theory one expects phonon sidebands at frequencies  $\pm \omega_0(T)$  in an inelastic scan at the superlattice positions. For  $T$  near  $T_c$ ,  $\omega_0(T) \rightarrow 0$ , and the sidebands collapse into a single overdamped peak centered at  $\omega = 0$ . Shapiro *et al.*<sup>9</sup> found such a central peak, which persisted with diminishing intensity at least  $70 \text{ }^\circ\text{C}$  above  $T_c$ , but no evidence for phonon sidebands at finite frequencies.

In the present experiments, a variety of inelastic scans (both with constant-energy and constant-momentum transfer) were made over a range of temperatures in the vicinity of those  $P$  points where strong superlattice reflections occur. All of these scans, some covering as much as 30 meV energy transfer, showed only the  $\omega = 0$  central peak. A typi-

cal scan is shown in Fig. 3. Under identical conditions, acoustical phonons were clearly visible. Thus, it can be stated with some confidence that, over a wide range of temperatures ( $0 < T < 950 \text{ }^\circ\text{C}$ ), there is no well-defined soft phonon at  $\bar{q}_p$  with an energy less than about 10 meV. The dominant fluctuation scattering associated with the transformation is therefore quasielastic in nature. The remainder of this study is directed toward the further characterization of this quasielastic scattering.

#### B. $Q$ dependence of the quasielastic scattering

The most characteristic and remarkable feature of the quasielastic scattering is that it is not localized in the vicinity of the  $P$  points, but instead lies along narrow rods in reciprocal space. One is of rods (which will be denoted type- $A$  rods) set parallel to  $[110]$  and the Miller indices of points on the rods satisfy  $h - k = \frac{1}{2}m$ ;  $l = \frac{1}{2}n$  where  $m$  and  $n$  are integers. Another are (type- $B$  rods) set related to the first by fourfold symmetry and have  $h + k = \frac{1}{2}m$ ,  $l = \frac{1}{2}n$ . Here and throughout this paper all coordinates refer to the HT rutile cell. Figure 2(b) shows two of the type- $B$  rods which lie in the experimental scattering plane. (The unconventional scattering plane was chosen to contain such rods of diffuse scattering.) The rods connect a series of equally spaced  $P$  points ( $\text{NbO}_2$  superlattice points) with  $R$  points ( $\text{VO}_2$  superlattice points) situated midway between them.

Figure 4 summarizes the variation of the scattered intensity along one such rod ( $h + k = \frac{3}{2}$ ,  $l = \frac{3}{2}$ ) as a function of temperature. The figure provides an accurate qualitative picture of the integrated quasielastic scattering. [In these scans the spectrometer was set to zero energy transfer, giving a bandpass of  $\sim 0.5 \text{ meV}$  [full width at half-maximum (FWHM)] about  $\omega = 0$ .

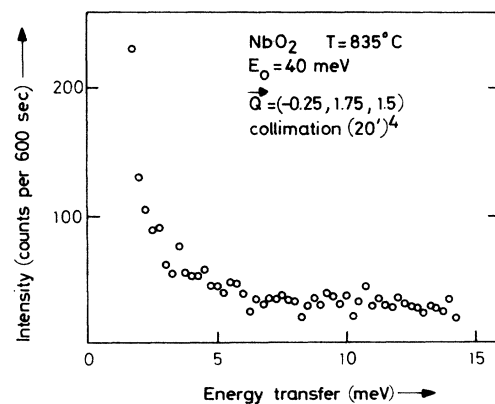


FIG. 3. Search for a soft-phonon mode at a  $P$  point.

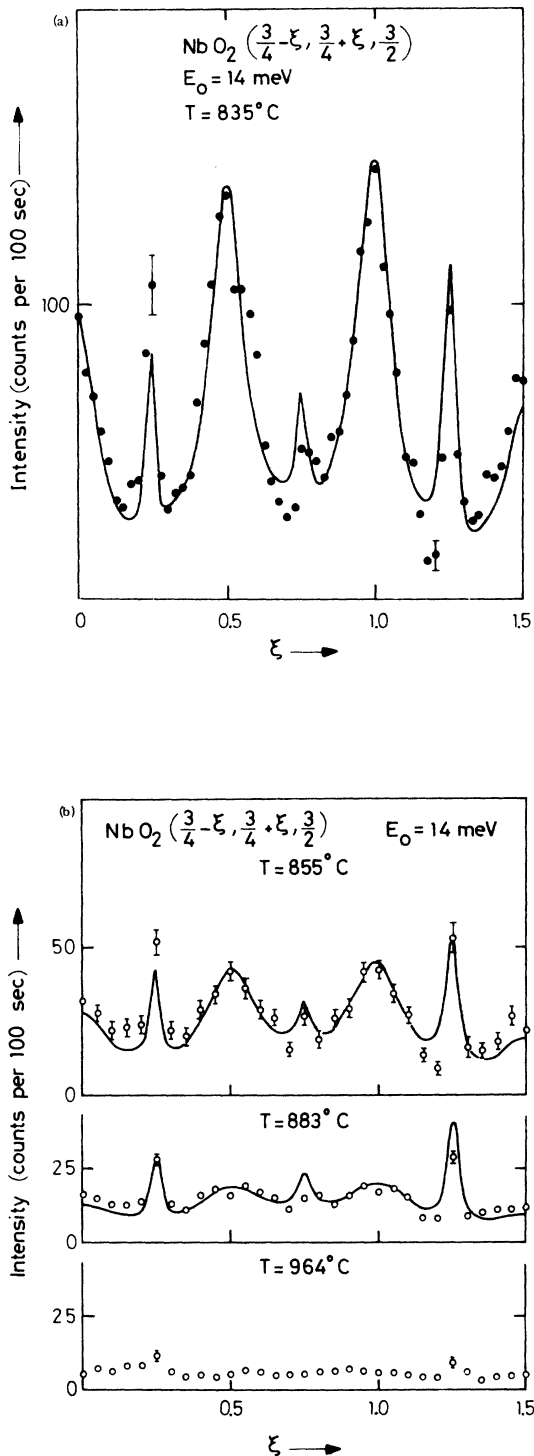


FIG. 4. Scans at zero-energy transfer along rods of critical scattering at various temperatures. Collimations for the experiments were 20'-20'-20'-20'. The lines in the figures are the results of the calculations described in the text.

This energy bandwidth is slightly too small to completely integrate the scattering, an effect which will be discussed in Sec. II C.) At the highest temperature,  $T = 964^\circ \text{C}$ , the intensity along the rod is roughly twice that of the background and rather featureless except for slight peaks at the  $R$  points  $\left[ \left( 1, \frac{1}{2}, \frac{3}{2} \right) \right]$  and  $\left( 2, -\frac{1}{2}, \frac{3}{2} \right)$  in particular]. As the temperature is lowered towards  $T_c$ , the general intensity level on the rod increases and additional modulation appears at the  $P$  points, and this grows to dominate the pattern near  $T_c$ . The peaks observed at the  $R$  point have a trivial explanation and do not, as might be supposed, arise from fluctuations into a  $\text{VO}_2$ -like stacking of (110) planes. As can be seen from Fig. 2(a), the  $R$  points represent points of intersection of the  $A$ - and  $B$ -type rods. Separate experiments which involved tilting the scattering plane slightly about the  $[1\bar{1}0]$  direction have established that the  $P$ -point intensity can be accounted for by a superposition of intensities from the two types of rods. This conclusion is also confirmed by a consideration of the relative intensities of the various  $R$ -point peaks (cf. Sec. III).

In order to examine the dependence of the scattering on momentum components perpendicular to the rod one should scan in two orthogonal directions, ideally along principle axes of the scattering which, on physical grounds, might be expected to correspond to  $[001]$  and  $[110]$  directions. As scans in these directions were incompatible with the scattering geometry, scans along two other orthogonal directions,  $[112]$  and  $[\bar{1}\bar{1}1]$ , were performed. The first of these is straightforward since  $[112]$  lies in the scattering plane. Consequently, such scans were performed at a number of temperatures at several positions along the rod. Results at both  $P$  and  $R$  points and between these positions are displayed in Fig. 5. Note that there is a definite narrowing of the peaks (most pronounced at the  $P$  points) as  $T_c$  is approached. The enhanced width at the  $R$  point is a result of the rod intersection described earlier.

Investigation of the  $Q$  width in the  $[\bar{1}\bar{1}1]$  direction was more difficult, as it involved using the goniometer-mount to manually tilt the sample out of the chosen scattering plane. For this reason the  $[\bar{1}\bar{1}1]$  scan was performed only at one temperature ( $827^\circ \text{C}$ ) near the  $\left( \frac{3}{4}, \frac{3}{4}, \frac{3}{2} \right)$   $P$  point. For this experiment the vertical resolution of the spectrometer was improved by introducing 40' vertical collimation (a Soller collimator with horizontal blades) before the detector. Even with this improvement one cannot expect accurate measurement of the  $[\bar{1}\bar{1}1]$   $Q$  width to be made with an instrument designed to scan only in two dimensions. In particular the vertical resolution is not well known and the intrinsic  $[\bar{1}\bar{1}1]$  width of the scattering would have to be large if it were to be unambiguously separated from the resolution width. The results of the  $[\bar{1}\bar{1}1]$  scan are shown in Fig. 6.

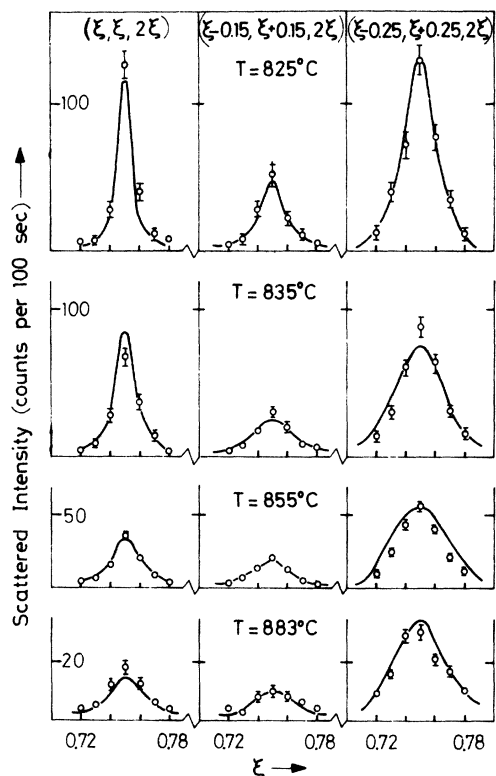


FIG. 5. Scans along  $\langle 112 \rangle$  at zero-energy transfer perpendicular to a rod of critical scattering. The incident neutron energy was 14 meV and collimations were 20'-20'-20'-20'. The lines in the figures are the result of the calculation described in the text. At each temperature, a single factor has been used to normalize the calculated curves to the data. The parameters used for the calculations are given in Table I except at  $T = 825^\circ\text{C}$  where we chose  $\kappa_{11} = 0.32$ ,  $\kappa_1 = 0.03$ ,  $\kappa_2 = 0.03$ . Since the widths of the peaks at  $T = 825^\circ\text{C}$  are dominated by instrumental resolution, the values of  $\kappa_1$  and  $\kappa_2$  are upper limits.

### C. Energy width of the quasielastic scattering

Preliminary low-resolution measurements indicated that the apparent energy width of the quasielastic scattering was greater than that expected from resolution effects alone. This was confirmed in a series of higher-resolution experiments which gave results of which Fig. 7 is typical. The widths are uniformly greater than the energy width of the resolution function (or to be more specific, greater than the FWHM,  $\Delta E = 0.32$  meV, of a vanadium scan). This fact, together with the obvious change of the observed widths with temperature, provides conclusive qualitative evidence for intrinsic energy width of the quasielastic scattering. However, the relative contributions of finite energy and momentum widths of the scattering of the measured energy width can only be assessed by detailed resolution calculations.

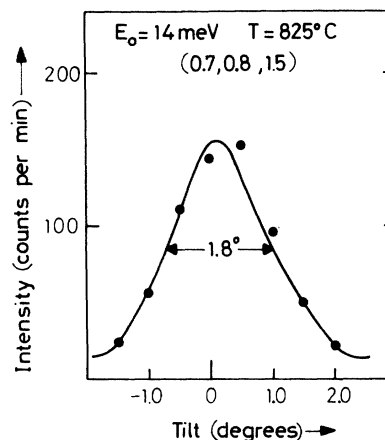


FIG. 6. Critical scattering close to a  $P$  point as a function of angle of tilt (about  $\langle \bar{1}10 \rangle$ ) of the scattering plane. The collimations for this experiment were (40'-20'-20'-open) with 40' vertical collimation before the detector. The curve through the data points is a guide to the eye.

## III. ANALYSIS AND DISCUSSION

### A. Form of the scattering cross section

In order to evaluate the data presented in Sec. II, it is necessary to establish a formalism which relates the diffuse-scattering cross section to the (time-dependent) atomic displacements,  $\bar{u}_{lk}(t)$ , which

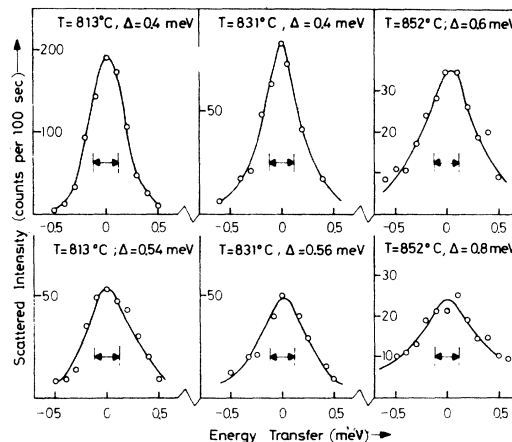


FIG. 7. Typical energy scans of the critical scattering. The incident neutron energy was 14 meV and collimations were 10'-20'-20'-10'. The upper row of scans was recorded at  $\bar{Q} = (0.75, 0.75, 1.5)$ , while the lower row was measured at  $\bar{Q} = (0.60, 0.90, 1.5)$ . The value of  $\Delta$  given on each figure is the measured FWHM of the scan. The resolution width indicated in the figures is essentially independent of temperature and has a value of 0.24 meV (FWHM).

comprise the critical fluctuations above  $T_c$ . To do this we first express the scattering cross section in terms of a time-dependent scattering amplitude  $F(\bar{Q}, t)$  as<sup>13</sup>

$$\frac{d^2\sigma}{d\omega d\Omega} = \int \langle F(\bar{Q}, t) F(-\bar{Q}, 0) \rangle_T e^{i\omega t} dt \quad (2)$$

For displacements which satisfy the condition  $\bar{Q} \cdot \bar{u}_{jk}(t) \ll 1$  one may write<sup>13</sup>

$$F(\bar{Q}, t) = \sum_{jk} b_k [\bar{Q} \cdot \bar{u}_{jk}(t)] e^{i\bar{Q} \cdot \bar{r}^{(jk)}} \quad (3)$$

where  $b_k$  is the scattering length (including the Debye-Waller factor) of the  $k$ th atomic species. The approximation  $\bar{Q} \cdot \bar{u}_{jk} \ll 1$  is well satisfied at  $\bar{Q}$  vectors of interest for the (static) displacements below  $T_c$  and we assume this to be true for the fluctuations above  $T_c$  as well. The displacements  $\bar{u}_{jk}(t)$  are related to fluctuations in the order parameters  $\sigma_\lambda(\bar{q}, t)$ , by equations analogous to Eq. (1). Thus,

$$\bar{u}_{jk}(t) = \sum_{q,\lambda} \sigma_\lambda(\bar{q}, t) \bar{e}_{k\lambda}(\bar{q}) e^{i\bar{q} \cdot \bar{r}_l} \quad (4)$$

The mode eigenvectors  $\bar{e}_{k\lambda}(\bar{q})$  are chosen to diagonalize the leading (quadratic) terms in a Landau expansion of the free energy.<sup>14</sup> They are thus the eigenvectors of the matrix

$$D_{\alpha\beta, k'k}(\bar{q}) = \sum_{ll'} \frac{\partial^2(\mathcal{F} - \mathcal{F}_0)}{\partial u_{\alpha, l'k} \partial u_{\beta, l'k'}} e^{i\bar{q} \cdot (\bar{r}_l - \bar{r}_{l'})} \quad (5)$$

where  $(\mathcal{F} - \mathcal{F}_0)$  is the free energy relative to the HT phase. The eigenvalues of  $\underline{D}(\bar{q})$  are the coefficients of the quadratic terms of the Landau expansion and represent generalized inverse susceptibilities. The above definition of the  $\bar{e}_{k\lambda}(\bar{q})$  guarantees the statistical independence of the modes (labeled by  $\lambda$ ) in the small-amplitude limit (truncation of the Landau expansion after the quadratic terms).

The analogy of the above equations with the conventional (harmonic) lattice dynamics is immediately apparent. In particular, the number and symmetry classification of the modes is identical to that of phonon modes. However, the exact form of the eigenvectors (to the extent that they are not completely determined by symmetry) may be different from the phonon eigenvectors and, of course, the mode dynamics may be very different. Here we shall be concerned only with the modes ( $\lambda = \lambda_A$  or  $\lambda_B$ ) associated with the lowest eigenvalue of the matrix  $\underline{D}(\bar{q})$ . It may be convenient to retain the terminology "soft-mode" to describe these modes. However, when used in this way, the term implies only divergent fluctuations and not (necessarily) a phonon frequency which tends to zero.

Turning once more to the evaluation of the diffuse-scattering cross section, we may combine Eqs. (2), (3), and (4) to give

$$\frac{d^2\sigma}{d\omega d\Omega} = \sum_{\lambda} |f_{\lambda}(\bar{Q})|^2 S_{\lambda}(\bar{Q}, \omega) \quad (6)$$

where

$$f_{\lambda}(\bar{Q}) = \sum_k b_k [\bar{Q} \cdot \bar{e}_{k\lambda}(\bar{Q})] e^{-i\bar{Q} \cdot \bar{r}_k} \quad (7)$$

specifies the coupling of the neutrons to the mode  $\lambda$ . The dynamics of the modes affect the cross section via the correlation function  $S_{\lambda}(\bar{Q}, \omega)$  which is given by

$$\begin{aligned} S_{\lambda}(\bar{Q}, \omega) &= \int dt \langle \sigma_{\lambda}(-\bar{Q}, t) \sigma_{\lambda}(\bar{Q}, 0) \rangle_T e^{i\omega t} \\ &= S_{\lambda}(\bar{Q}) F_{\lambda}(\bar{Q}, \omega) \end{aligned} \quad (8)$$

In writing Eq. (6) we have assumed that modes are statistically independent<sup>15</sup> so that

$$\langle \sigma_{\lambda} \sigma_{\lambda'} \rangle_T \sim \delta_{\lambda\lambda'}$$

Integrating Eq. (6) over  $\omega$  one finds that

$$\frac{d\sigma}{d\Omega} = \sum_{\lambda} |f_{\lambda}(\bar{Q})|^2 S_{\lambda}(\bar{Q}) \quad (9)$$

where

$$S_{\lambda}(\bar{Q}) = \int d\omega S_{\lambda}(\bar{Q}, \omega) = \langle \sigma_{\lambda}(\bar{Q}, 0) \sigma_{\lambda}(-\bar{Q}, 0) \rangle \quad (10)$$

is the equal-time correlation function for the fluctuations.

In the absence of a detailed microscopic theory neither  $\underline{D}(\bar{q})$  nor its eigenvectors  $\bar{e}_{k\lambda}(\bar{q})$  are known. All that can be done is to replace  $\bar{e}_{k\lambda_A}(\bar{q})$  by  $\bar{E}_k(\bar{q}_A)$  and  $\bar{e}_{k\lambda_B}(\bar{q})$  by  $\bar{E}_k(\bar{q}_B)$ , where  $\bar{E}_k(\bar{q}_A)$  and  $\bar{E}_k(\bar{q}_B)$  are the polarization vectors of the condensed displacements below  $T_c$ , determined from our earlier diffraction study [see Eqs. (15) and (16) and Tables I and III of Ref. 7]. This replacement should be correct at  $\bar{q} = \bar{q}_A$  or  $\bar{q}_B$  and we can argue that it will introduce little error at other wave vectors. The argument is as follows. The  $\bar{E}(\bar{q}_A)$  displacements shown in Fig. 1 can be characterized as a dimerization along the  $z$  axis of Nb ( $A$ ) atoms together with atomic motions which tend to maintain constant metal-oxygen near-neighbor distances. While these considerations suffice to relate qualitatively the displacements within a given (110) plane (the shaded one in Fig. 1, for example), they do not provide a natural coupling mechanism between adjacent (110) planes. Thus we expect that  $\bar{e}_{k, \lambda_A}(\bar{q})$  will be only weakly dependent on components of  $\bar{q}$  perpendicular to the (110) planes [i.e.,  $\bar{q} = \bar{q}_A + (\epsilon, \epsilon, 0)$ ]. However, for  $\bar{q}$  within a (110) plane we expect that  $\bar{e}_{k, \lambda_A}(\bar{q})$  may change rapidly with  $\bar{q}$ . Translating these observations into the language of Sec. II, one finds that  $\bar{e}_{k, \lambda}(\bar{q})$  is expected to vary slowly along the rods of diffuse scattering but rapidly

perpendicular to the rods. Since the rods are relatively thin the rapid variation of  $\bar{e}_{k,\lambda}(\bar{q})$  perpendicular to a rod is of little practical consequence and our replacement of the mode eigenvectors by  $\bar{E}_\lambda(\bar{q}_A)$  and  $\bar{E}_\lambda(\bar{q}_B)$  should be a reasonable approximation.

The form factors  $f_\lambda(\bar{Q})$  defined by Eq. (7) can, with the replacement discussed above, be evaluated from the low-temperature distortion determined by our earlier diffraction study.<sup>7</sup> In order to specify the scattering cross section Eq. (6) one needs, in addition, a form for the fluctuation spectrum  $S_\lambda(\bar{Q}, \omega)$  and information about the Debye-Waller factor. A general form for the static susceptibility  $\chi_\lambda(\bar{Q})$  is derived in the Appendix [Eq. (A11)] and this has been used to calculate  $S_\lambda(\bar{Q})$  via the fluctuation-dissipation theorem. Specifically we have used

$$S_\lambda(\bar{Q}) = \frac{C(T)}{1 + (\sin \xi_{\parallel}/\kappa_{\parallel})^2 + (\sin \xi_{\perp}/\kappa_{\perp})^2 + (\sin \xi_z/\kappa_z)^2}, \quad (11)$$

where  $C(T)$  is a temperature-dependent constant determined by normalizing to the data and

$$\begin{aligned} \xi_{\parallel} &= \frac{1}{2}(q_x \pm q_y)a, & \xi_{\perp} &= \frac{1}{2}(q_x \mp q_y)a - \frac{1}{2}\pi, \\ \xi_z &= q_z c - \pi, \end{aligned} \quad (12)$$

where upper signs refer to the  $A$  mode and lower ones to the  $B$  mode.  $S_\lambda(\bar{Q})$  is thus specified in terms of three inverse correlation lengths:  $\kappa_{\parallel}$ , which determines the width of a  $\bar{q}_\rho$  peak in a direction parallel to the rod of scattering and  $\kappa_z$  and  $\kappa_{\perp}$  which control widths perpendicular to the rods in the  $z$  direction and in the  $x$ - $y$  plane. At a later stage of data analysis we shall include the frequency dependence of  $S(\bar{Q}, \omega)$  as a peak of width  $\Delta(\bar{Q})$  centered at  $\omega = 0$ . The final quantity needed for the evaluation of Eq. (6) is the Debye-Waller factor. In our diffraction study<sup>7</sup> of the LT phase of  $\text{NbO}_2$ , Debye-Waller parameters were obtained at room temperature. Since Bragg reflections which are common to the LT and HT phases showed relatively little temperature dependence,<sup>7,12</sup> it is reasonable to assume that the Debye-Waller factors are themselves independent of temperature.

## B. Calculations

In order to determine the values of the parameters  $\kappa_{\parallel}$ ,  $\kappa_{\perp}$ , and  $\kappa_z$  which best describe the data at each temperature it is necessary to convolve the proposed fluctuation spectrum with the instrumental resolution of the three-axis spectrometer used in this study. A standard program<sup>16</sup> has been used to perform this convolution in the elastic approximation, i.e., with  $F(\bar{Q}, \omega) = \delta(\omega)$ . To understand the nature of this approximation let us denote by  $N(\bar{Q}_0)$  the true spectrometer counting rate at some nominal setting  $\bar{Q}_0$  and

at  $\omega_0 = 0$ . Further, let  $N_0(\bar{Q}_0)$  be the counting rate calculated in the elastic approximation. The ratio of  $N$  and  $N_0$  depends upon the inelasticity through the expression

$$\frac{N(\bar{Q}_0)}{N_0(\bar{Q}_0)} = \int F(\bar{Q}_0, \omega) g(\bar{Q}_0, \omega) d\omega, \quad (13)$$

where  $g(\bar{Q}_0, \omega)$  is defined by

$$N_0(\bar{Q}_0)g(\bar{Q}_0, \omega) \equiv \int d\bar{Q} R(\bar{Q} - \bar{Q}_0, \omega) S(\bar{Q}) \quad (14)$$

and  $R(\bar{Q} - \bar{Q}_0, \omega)$  is the instrumental response function. In deriving Eq. (13) we have assumed that  $F(\bar{Q}, \omega)$  varies so slowly within the instrumental response that it can be replaced by  $F(\bar{Q}_0, \omega)$ . By direct calculation it can be shown that for a wide range of values of  $\kappa_{\parallel}$ ,  $\kappa_{\perp}$ , and  $\kappa_z$  and for experimental conditions relevant to Figs. 4–6, the energy width ( $\Delta_R$ ) of  $g(\bar{Q}_0, \omega)$  is essentially independent of  $\bar{Q}_0$ . Thus, the ratio  $N(\bar{Q}_0)/N_0(\bar{Q}_0)$  is constant except for the  $\bar{Q}$  dependence of the energy width of  $F(\bar{Q}_0, \omega)$ . The latter is given by  $(\Delta^2 - \Delta_R^2)^{1/2}$  where  $\Delta$  is the observed energy width. For the experimental conditions of Figs. 4–6 the variation of the observed energy width along the rod of critical scattering is negligible at  $T = 830^\circ\text{C}$  but may be  $\pm 15\%$  for temperature of  $850^\circ\text{C}$  and above. The effect of this variation is difficult to include (because our measurements of the energy widths at the resolution appropriate to Figs. 4–6 are not sufficiently extensive or accurate) and we have ignored it in these calculations. However, inclusion of the effect would often lead to improved agreement with experiment. For example, for  $\xi \sim 0.15$  at  $T = 855^\circ\text{C}$  the calculated curve in Fig. 4 is brought into agreement with the data when variation of the energy width is accounted for.

Rather than attempt a complicated least-squares-fitting procedure which would have given little insight into the effect of various parameters on the calculated intensities, we have estimated the inverse correlation lengths by a trial and error method. This procedure has allowed us to draw the following conclusions: (i) The effect of varying the sample mosaic within reasonable limits ( $20' - 30'$ ) is negligible even for scans like those displayed in Fig. 4. (ii) The Debye-Waller factor produces a 20% reduction of intensity at  $\xi = 0$  in Fig. 4 and a 30% reduction at  $\xi = 1.5$ . (iii) The widths of the  $R$ -point peaks at  $\xi = 0.25$  and  $\xi = 1.25$  in Fig. 4 dictate that  $\kappa_{\perp} \leq 0.06$  at all temperatures. Variation of  $\kappa_{\perp}$  has a pronounced effect on the intensity of the  $R$ -point peaks and, in our calculations, the value of  $\kappa_{\perp}$  has been chosen to fit the intensities of these peaks.  $\kappa_{\perp}$  also has an effect on the tilt profile shown in Fig. 6. However, this profile could not be fitted with acceptable values of  $\kappa_{\perp}$  and the nominal spectrometer collimations, etc. The final parameter set

(see Table I) for  $T = 835^\circ\text{C}$  gives a width for the tilt profile of  $1.3^\circ$  compared to a measured width of  $1.8^\circ$ . In view of the gross uncertainties in the specification of vertical resolution of the spectrometer, we do not regard this discrepancy as too important. (iv) The widths of the (112) scans shown in Fig. 5 are independent of  $\kappa_{\parallel}$  at  $\bar{Q} = (0.75, 0.75, 1.5)$  and only weakly affected by the value of  $\kappa_{\parallel}$  at the other points of measurement. Variation of  $\kappa_{\perp}$  within acceptable limits (i.e.,  $\kappa_{\perp} \leq 0.06$ ) has little effect on the widths of the peaks in Fig. 5: these widths essentially determine values for  $\kappa_z$ . (v) The parameter  $\kappa_{\parallel}$  is determined by the widths of the  $P$ -point peaks shown in Fig. 4.

The parameters, which give a good overall description of the data, have been used to generate the solid curves in Figs. 4 and 5 (but not Fig. 6) and are listed in Table I. Since the data are, in general, well represented by the calculations, we find no cause to be dissatisfied with the form chosen for the scattering cross section. In particular, since the relative intensities of the various peaks in Fig. 4 are well reproduced, the form chosen for  $f_{\lambda}(\bar{Q})$  appears to be essentially correct. For the reasons discussed earlier the values obtained for the  $\kappa$ 's should not be overinterpreted. Nevertheless, a number of qualitative observations can probably be made. For example, the planar correlations ( $\kappa_{\perp}$  and  $\kappa_z \ll \kappa_{\parallel}$ ) discussed earlier are evident as is the departure from the mean-field behavior  $\kappa_{\parallel}^2 \propto |T - T_c|$ .

When the values of the  $\kappa$ 's are used to determine the energy resolution at different points along rods of critical scattering, the results are found to depend very little on the values of the correlation lengths. Indeed, for all of the data of Fig. 7, the instrumental resolution is  $\Delta_R = 0.25$  meV, a value which is, as expected, slightly less than the width (0.32 meV) of a vanadium scan. From Fig. 7 we may draw several conclusions. (i) The intrinsic energy width [i.e.,  $(\Delta^2 - \Delta_R^2)^{1/2}$ ] of the critical scattering is finite and easily measurable even at reduced temperature  $|T - T_c|/T_c$  of order  $10^{-3}$ . See, however, point (iii) below ( $T_c = 808.5^\circ\text{C}$  for this sample). (ii) The energy width is  $Q$  dependent, being smaller at the  $P$  point than at neighboring

points along the rod of critical scattering. (iii) Both at the  $P$  point (upper set of profiles) and between  $P$  and  $R$  points (lower set of profiles) the energy width decreases as the transition is approached. The finite width at the  $P$  point near  $T_c$ , apparently at odds with the concept of critical slowing down, may well be an artifact of finite  $Q$  resolution. Qualitatively the behavior of the energy width is roughly consistent with that of an overdamped phonon mode, but we emphasize that there is no evidence for a soft phonon branch from which it evolves.

#### IV. CONCLUDING REMARKS

In a recent paper, Tolédano and Tolédano<sup>17</sup> (TT) call attention to the fact that the present interpretation of the NbO<sub>2</sub> transformation in terms of order parameters with wave vectors  $\{\bar{q}_p\}$  contradicts the Landau-Lifschitz criterion that the order parameter should not have symmetry properties that include a totally symmetric antisymmetrized product representation  $\{\Gamma\}^2$ . These authors postulate that this difficulty is removed if the transformation from HT rutile to LT bct structure proceeds through an intermediate structure involving displacements with wave vector  $\{\bar{q}_M\} = \{\frac{1}{2}, \frac{1}{2}, 0\}$ . As the support for this conjecture they quote the powder x-ray results of Sakata *et al.*<sup>3</sup> which show apparent weak superstructure peaks which persist some  $100^\circ\text{C}$  above the acknowledged transformation temperature of  $\sim 800^\circ\text{C}$ .

It seems clear to us that this proposal must be rejected. The original single-crystal neutron diffraction results of Shapiro *et al.*<sup>9</sup> show clearly that the Bragg intensities at the  $(\frac{1}{2}, \frac{1}{2}, 0)$  points vanish along with the primary reflections at  $(\frac{1}{4}, \frac{1}{4}, \frac{1}{2})$  at  $T_c \approx 808^\circ\text{C}$ . Moreover, it seems quite likely that the weak powder diffraction peaks observed by Sakata *et al.*<sup>3</sup> are in fact the diffuse scattering described in the present study. The diffuse character of the scattering is much less apparent in the powder diffraction technique. We know of no other evidence for an intermediate phase in the region  $800 \sim 900^\circ\text{C}$ .

The basic objection raised by TT, which was first noted by Mukamel,<sup>18</sup> remains. The restriction on  $\{\Gamma\}^2$  ensures by symmetry that the Landau expansion of the free energy has an extremum at the proper wave vector ( $\{\bar{q}_p\}$  in the present case). The problem is therefore precisely the one discussed in more physical terms by Pynn and Axe,<sup>12</sup> and again in this work. Namely, there is no symmetry argument that singles out the wave vector  $(\frac{1}{4}, \frac{1}{4}, \frac{1}{2})$  over the more general value  $(\zeta, \zeta, \frac{1}{2})$ . On the other hand, the behavior of the diffuse scattering shows unambiguously that the instability does develop at, or at least very near  $\{q_p\}$ . Furthermore, the discussion, particularly in the Appendix of this paper, has attempted to clarify the kinds

TABLE I. Fitted values of the parameters  $\kappa_{\parallel}$ ,  $\kappa_{\perp}$ , and  $\kappa_z$  at various temperatures. The uncertainties in the values of  $\kappa_{\perp}$  and  $\kappa_z$  are about  $\pm 0.01$ . For  $\kappa_{\parallel}$ , the random error is about  $\pm 0.05$ ; however, there is an additional systematic error (see Sec. III B) which increases with temperature from  $\sim 0$  at  $835^\circ\text{C}$  to  $\sim 15\%$  at  $883^\circ\text{C}$ .

$T$ ( $^\circ\text{C}$ )	$\kappa_{\parallel}$	$\kappa_{\perp}$	$\kappa_z$
835	0.32	0.03	0.05
855	0.55	0.05	0.025
883	0.87	0.06	0.025

of physical assumptions necessary to produce an "accidental" minimum in the free energy near  $\{\bar{q}_\rho\}$ . Once this key physical point is accepted then the Landau-Lifshitz criterion becomes inappropriate either because (a) the wave vector of the condensed displacements is initially very slightly different from  $\{\bar{q}_\rho\}$  subsequently locking on to that value, or (b) the transformation locks directly onto  $\{q_\rho\}$  but is very slightly first order.

Sladek and Bennett<sup>19</sup> have compared the Debye  $\Theta$  obtained by low-temperature specific-heat measurements with that derived from low-temperature ultrasonic measurements and find the former to be  $\sim 5\%$  lower. They suggest that the discrepancy is due to an increased density of phonon states with acoustical-like dispersion, which represent a special kind of "soft mode" termed variously "phasons" or "sliding modes." (Note however that the gapless nature of phason excitations is conventionally associated with incommensurate structures.)

It would be somewhat surprising and very interesting if the presence of such excitations could be verified directly at low temperatures, especially in view of the fact that at room temperature and above only diffusive quasielastic excitations were found in this study. Indeed, such diffuse modes, if they persist to low temperatures, could *in principle* explain the discrepancy observed by Sladek and Bennett; there is no *a priori* need to introduce further propagating modes.

#### ACKNOWLEDGMENTS

Work at Brookhaven was supported by the U. S. ERDA under Contract No. EY-76-C-02-0016. One of us (P.M.R.) was supported in part by U. S. Army Contract No. DAAG 2977 G0084.

#### APPENDIX: MEAN-FIELD MODEL OF THE FLUCTUATIONS

We suppose that for a discussion of the fluctuations in the HT phase the Hamiltonian can be approximated by

$$\mathcal{H} = -\frac{1}{2} \sum_{\bar{q}, \lambda} v_\lambda(\bar{q}) \sigma_\lambda(\bar{q}) \sigma_\lambda(-\bar{q}) - \sum_{\bar{q}} h_\lambda(\bar{q}) \sigma_\lambda(-\bar{q}) \quad (\text{A1})$$

where the first term is diagonal in  $\lambda$  because of our choice of mode eigenvectors [cf. Eq. (4)] and  $h_\lambda(\bar{q})$  is a fictitious conjugate field introduced to facilitate the discussion of a generalized susceptibility. By familiar arguments the self-consistent solutions for  $\sigma_\lambda(\bar{q})$  in the mean-field approximation (MFA) in the limit  $\sigma_\lambda(\bar{q}) \rightarrow 0$  are of the form

$$\sigma_\lambda(\bar{q}) = \chi_0 [v_\lambda(\bar{q}) \sigma_\lambda(\bar{q}) + h_\lambda(\bar{q})] \quad (\text{A2})$$

where  $\chi_0 = C/T$  and  $C$  is constant. By definition the order-parameter susceptibility is

$$\chi_\lambda(\bar{q}) \equiv \sigma_\lambda(\bar{q}) / h_\lambda(\bar{q}) = \chi_0 / [1 - v_\lambda(\bar{q}) \chi_0] \quad (\text{A3})$$

and we can relate  $\chi_\lambda(\bar{q})$  to  $\langle \sigma_\lambda(\bar{q}) \sigma_\lambda(-\bar{q}) \rangle$  through the fluctuation-dissipation theorem<sup>13</sup>

$$\langle \sigma_\lambda(\bar{q}) \sigma_\lambda(-\bar{q}) \rangle = kT \chi_\lambda(\bar{q}) \quad (\text{A4})$$

$\chi_0(T)$  can be evaluated through the condition that  $\chi_\lambda(\bar{q}_\rho)$  must diverge at  $T_c$ , i.e.,

$$v_\lambda(\bar{q}_\rho) \chi_0(T_c) = 1 \quad (\text{A5})$$

In order to facilitate the construction of an interaction potential  $v_\lambda(\bar{q})$  with the correct qualitative features consider a direct-space description of the form

$$v_\lambda(\bar{q}) = \frac{1}{N} \sum_{\bar{l}, \bar{l}'} v_\lambda(\bar{l} - \bar{l}') e^{-i\bar{q} \cdot (\bar{l} - \bar{l}')} \quad (\text{A6})$$

We have examined in detail a model with the following intercell potentials:

$$v_\lambda(\bar{l} - \bar{l}') \equiv v_\lambda(\alpha\beta\gamma) \quad ,$$

where  $\alpha\bar{a} + \beta\bar{b} + \gamma\bar{c}$  is a direct lattice vector. (a)  $v_\lambda((0, 0, 1)) \equiv v_z \ll 0$  to account for the strong tendency toward antiferrodistortive (AFD) dimerization along  $\bar{c}$ . (b)  $v_\lambda((1, 1, 0)) \neq v_\lambda((1, \bar{1}, 0))$ . The inequality is crucial and results from the lack of a simple fourfold rotation axis. From an inspection of Fig. 1, we expect that  $v_A((1, \bar{1}, 0)) \equiv v_{\perp} \ll 0$  to account for the AFD tendency in this direction. We shall see that  $v_A((1, 1, 0)) \equiv v_{\parallel}$  must be positive to account for the LT NbO<sub>2</sub> structure, but from Fig. 1 it is only possible to guess that  $|v_{\perp}| \ll |v_{\parallel}|$ . The fourfold screw axis interchanges sublattices  $A$  and  $B$  so that  $v_B((1, 1, 0)) = v_{\parallel}$  and  $v_B((1, \bar{1}, 0)) = v_{\perp}$ . (c) Finally for completeness we include  $v_\lambda((1, 0, 0)) = v_\lambda((0, 1, 0)) \equiv v_x$ . The equality in this case follows from the presence of (110) mirror planes. Although it is difficult to make an *a priori* guess as to its magnitude, we shall see that both the distribution of diffuse scattering and the LT structure suggest that  $v_x \approx 0$ .

Performing the summation in Eq. (A6) for  $\lambda = A$ , we find

$$v_A(\bar{q}) = 2[v_z \cos \phi_z + v_{\parallel} \cos(\phi_x - \phi_y) + v_{\perp} \cos(\phi_x + \phi_y) + v_x (\cos \phi_x + \cos \phi_y)] \quad (\text{A7})$$

where  $\phi_x = q_x a$ ,  $\phi_y = q_y a$ , and  $\phi_z = q_z c$ . It is convenient to shift the origin to  $\bar{q}_A = (\frac{1}{4}, -\frac{1}{4}, \frac{1}{2})$  by the transformation

$$\begin{aligned}
 (\phi_x, \phi_y, \phi_z) &\equiv (q_x a, q_y a, q_z c) \\
 &= \left( \frac{1}{2} \pi + \xi_{\parallel} + \xi_{\perp}; -\frac{1}{2} \pi + \xi_{\parallel} - \xi_{\perp}; \pi + \xi_z \right),
 \end{aligned}
 \tag{A8}$$

where  $\xi_{\parallel}$  is along the rod of diffuse scattering arising from the  $A$  sublattice and  $\xi_{\perp}$  and  $\xi_z$  are perpendicular to the rod. Then,  $v_A(\bar{q})$  becomes

$$\begin{aligned}
 v_A(\bar{q}) &= -2v_z \cos \xi_z - 2v_{\parallel} \cos 2\xi_{\perp} \\
 &\quad + 2v_{\perp} \cos 2\xi_{\parallel} - 4v_x \sin \xi_{\perp} \cos \xi_{\parallel}.
 \end{aligned}
 \tag{A9}$$

For the instability to occur at  $\bar{q}_A$  it is only necessary that  $v_A(\bar{q})$  be maximized at  $\bar{q}_A$ , i.e., for

$$\xi_{\parallel} = \xi_{\perp} = \xi_z = 0.$$

Neglecting for the moment the last term in Eq. (A9), this condition is met if we add to the constraints on the parameters in  $v_A(\bar{q})$  discussed above the requirement that  $v_{\perp} > 0$ . [If  $v_{\perp} < 0$  the maximum of  $v_A(\bar{q})$  shifts to  $\xi_{\parallel} = \frac{1}{2}\pi$ , i.e., to  $\bar{q}_R = (\frac{1}{2}, 0, \frac{1}{2})$ . Obviously within this model the nearly equal stability of NbO<sub>2</sub>-like and VO<sub>2</sub>-like distortions, as well as the strongly anisotropic diffuse scattering, are expressed through the condition that  $|v_{\perp}|/|v_{\parallel}| \ll 1$ .] Since the last term in Eq. (A9) is odd in  $\xi_{\perp}$  it moves the minimum of  $v_A(\bar{q})$  to a finite value of  $\xi_{\perp}$ . This is a manifestation of the previously noted fact<sup>12</sup> that  $\bar{q}_A = (\frac{1}{4}, \frac{1}{4}, \frac{1}{2})$  has no unique symmetry which distinguishes it from other wave vectors on the line  $(\zeta, \zeta, \frac{1}{2})$ . Higher order "umklapp" terms in the free energy are capable of causing a "locking on" to  $\zeta = \frac{1}{4}$  if the maximum of  $v_A(\bar{q})$  is nearby, but this requires that the transformation be

discontinuous (1st order). We have observed no such discontinuity and furthermore the diffuse scattering maximizes at or very near  $\zeta = \frac{1}{4}$ . We therefore believe that the occurrence of the instability at  $\zeta = \frac{1}{4}$  is "accidental" in the symmetry sense, or, within the context of this model, that  $v_x$  is very small. We therefore set  $v_x$  equal to zero.

Having assured that  $v_A(\bar{q})$  is maximized at  $\bar{q}_A$  we may rewrite the susceptibility as

$$\chi_A(\bar{q}) = \chi_A(\bar{q}_A) \left/ \left[ 1 + \left( \frac{T_c}{T - T_c} \right) \left( \frac{v_A(\bar{q}_A) - v_A(\bar{q})}{v_A(\bar{q}_A)} \right) \right] \right.
 \tag{A10}$$

$$\chi_A(q) = \chi_A(\bar{q}_A) \left/ \left[ 1 + \frac{\sin^2 \frac{1}{2}(\xi_z)}{\kappa_z^2} + \frac{\sin^2 \xi_{\parallel}}{\kappa_{\parallel}^2} + \frac{\sin^2 \xi_{\perp}}{\kappa_{\perp}^2} \right] \right.,
 \tag{A11}$$

where  $\chi_A(\bar{q}_A)$ , the divergent susceptibility, is

$$\chi_A(\bar{q}_A) = [v_A(\bar{q}_A)]^{-1} T_c / (T - T_c) \tag{A12}$$

and

$$\begin{aligned}
 \kappa_z^2 &= [(v_z + v_{\parallel} - v_{\perp})/2v_z] (T - T_c) / T_c, \\
 \kappa_{\parallel}^2 &= [(v_z + v_{\parallel} - v_{\perp})/2v_{\parallel}] (T - T_c) / T_c, \\
 \kappa_{\perp}^2 &= [(-v_z - v_{\parallel} + v_{\perp})/2v_{\perp}] (T - T_c) / T_c.
 \end{aligned}
 \tag{A13}$$

Note that the three inverse correlation lengths are constrained by the relation

$$(\kappa_z^2)^{-1} + (\kappa_{\parallel}^2)^{-1} + (\kappa_{\perp}^2)^{-1} = 2[T_c / (T - T_c)] \tag{A14}$$

\*Present address: Institute Laue-Langevin, Avenue des Martyrs 156 X, 38042 Grenoble Cedex, France.

<sup>1</sup>A recent review of the properties of VO<sub>2</sub> together with various attempts at their theoretical description has been given by A. Zylbersztein and N. F. Mott, Phys. Rev. B **11**, 4383 (1975).

<sup>2</sup>R. F. Jannick and D. H. Whitmore, J. Phys. Chem. Solids **27**, 1183 (1966).

<sup>3</sup>T. Sakata, K. Sakata, and I. Nishida, Phys. Status Solidi **20**, K155 (1967); K. Sakata, J. Phys. Soc. Jpn. **26**, 582 (1969); **26**, 867 (1969).

<sup>4</sup>P. M. Raccach, G. Belanger, J. Destry, G. Perluzzo, and P. M. Raccach, Can. J. Phys. **52**, 2272 (1974).

<sup>5</sup>G. Andersson, Acta Chem. Scand. **10**, 623 (1956).

<sup>6</sup>B. O. Marinder, Ark. Kemi **19**, 435 (1963).

<sup>7</sup>R. Pynn, J. D. Axe, and R. Thomas, Phys. Rev. B **13**, 2965 (1976).

<sup>8</sup>J. D. Axe, R. Pynn, and R. Thomas, Proceedings of Puerto Rico Conference, 1975 (unpublished).

<sup>9</sup>S. M. Shapiro, J. D. Axe, G. Shirane, and P. M. Raccach, Solid State Commun. **15**, 377 (1974).

<sup>10</sup>J. R. Brews, Phys. Rev. B **1**, 2557 (1970).

<sup>11</sup>F. H. Pollack, J. B. Miestein, and P. M. Raccach, Bull. Am. Phys. Soc. **18**, 370 (1973).

<sup>12</sup>R. Pynn and J. D. Axe, J. Phys. C **9**, L199 (1976).

<sup>13</sup>W. Marshall and S. W. Lovesey *Theory of Thermal Neutron Scattering* (Oxford U. P., New York, 1971).

<sup>14</sup>L. D. Landau and E. M. Lifshitz, *Statistical Physics* (Pergamon, New York, 1958).

<sup>15</sup>Note that below  $T_c$  there is a well-defined phase relation between condensed  $\lambda_A$  and  $\lambda_B$  displacements due to anharmonic terms in the Landau free energy (see Ref. 7). The effects of such terms on the critical scattering, which may be significant close to  $T_c$ , are ignored in this paper.

<sup>16</sup>See, for example, R. Pynn, *Methods of Computational Physics* (Academic, New York, 1976), and references cited therein.

<sup>17</sup>P. Tolédano and J. C. Tolédano, Phys. Rev. B **16**, 386 (1977).

<sup>18</sup>D. Mukamel and S. Krinsky, Phys. Rev. B **13**, 5065 (1976).

<sup>19</sup>J. G. Bennett and R. J. Sladek, Bull. Am. Phys. Soc. **22**, 474 (1977).

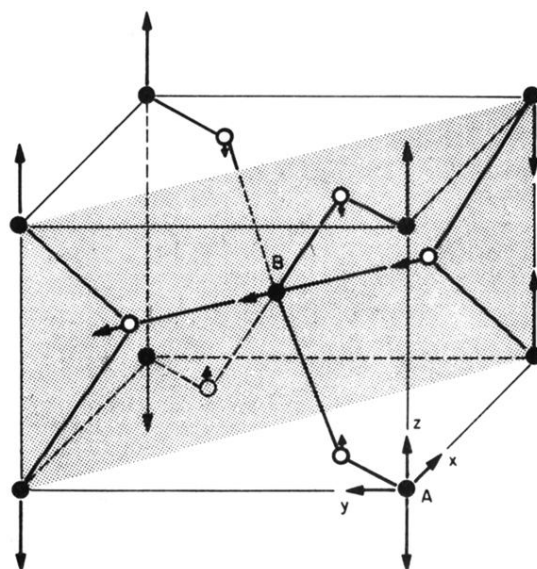


FIG. 1. High-temperature unit cell of  $\text{NbO}_2$  with the displacements due to the  $\bar{q}_A$  distortion indicated by arrows. The *A* and *B* metal sublattices are indicated. (●, Nb; ○, oxygen)